Improving the quality of deep-tissue elastography imaging: A Kelvin–Voigt model-based and multi-point denoising approach

Nguyen Sy Hiep[1,2], Luong Quang Hai[3], Tran Duc Tan[4],
Pham Van Tang[5], Tran Duc Nghia[6*]

[1]Graduate University of Science and Technology, Vietnam Academy of Science and Technology, 18 Hoang Quoc Viet, Nghia Do, Hanoi, Vietnam;
[2]Thai Nguyen University of Information and Communication Technology, Z115 Street, Quyet Thang, Thai Nguyen, Vietnam;
[3]Department of Biomedical Engineering, Le Quy Don Technical University, 236 Hoang Quoc Viet, Nghia Do, Hanoi, Vietnam;
[4]Faculty of Electrical and Electronic Engineering, Phenikaa School of Engineering, Phenikaa University, Nguyen Trac, Duong Noi,Hanoi, Vietnam;
[5]Faculty of Basic Sciences, Military Logistics Academy, Bo De, Hanoi, Vietnam;
[6]Institute of Information Technology, Vietnam Academy of Science and Technology, 18 Hoang Quoc Viet, Nghia Do, Hanoi, Vietnam.
[*]Corresponding author: nghiatd@ioit.ac.vn
Received 17 Oct. 2025; Revised 06 Feb. 2026; Accepted 10 Apr. 2026; Published 25 Apr. 2026.
DOI: https://doi.org/10.54939/1859-1043.j.mst.110.2026.34-44

ABSTRACT

Tissue stiffness has been recognized as an important indicator of pathological conditions. Ultrasound elastography, which relies on the mechanical stiffness properties of tissue, has proven effective in diagnosing various Malignant conditions like breast cancer, thyroid disorders, prostate abnormalities. With advantages including speed, low cost, non-invasiveness, and reliability, elastography has gained significant attention and is now widely applied in clinical diagnostics. However, this technique faces challenges in deep tissue regions, where increased noise and shear wave attenuation lead to degraded image quality and reduced diagnostic accuracy. To address these limitations, this study proposes an integrated approach combining LMS filtering, median filtering, and enhanced multi-source excitation to improve the signal-to-noise ratio (SNR) and enhance image quality in deep tissues. The effectiveness of the proposed method is evaluated using RMSE and Q-index metrics, demonstrating significant noise reduction and improved diagnostic reliability.

Keywords: AHI algorithm; LMS filter; Elastography image; Median filter; Multi-point excitation.

1. INTRODUCTION

Cancer is one of the most serious health issues today, placing a heavy burden on families and society due to high treatment costs and high mortality rates [1–3]. According to the Global Cancer Report 2022 from the International Agency for Research on Cancer (IARC), there were about 20 million new cancer cases and 10 million deaths worldwide [4]. In the same year, Vietnam recorded approximately 182,000 new cases and 120,000 deaths from cancer. Research has shown that early detection can significantly improve survival rates and reduce treatment costs [5–7]. Early diagnosis through routine health screenings plays a critical role in improving the effectiveness of cancer treatment. However, more than half of cancer patients are still detected only when the disease has progressed to an advanced stage. Early diagnosis through routine health screenings plays a critical role in improving the effectiveness of cancer treatment. However, more than half of cancer patients are still detected only when the disease has progressed to an advanced stage [8]. The main reasons include high screening costs (such as SPECT or PET-CT), long scanning times (MRI), or worries about radiation exposure (X-ray, CT). Because of these limitations, tissue elastography ultrasound has gained increasing attention. It's a non-invasive, affordable, safe, and fast imaging technique

with high diagnostic accuracy [9-10]. In a study by Youssef Ahmed Youssef Selim *et al.* [11], involving 6,200 lesions (45% benign and 55% malignant), elastography achieved 90% sensitivity, 86% specificity, and an AUC of 0.92, confirming its strong effectiveness in cancer diagnosis. Elastography imaging faces challenges such as noise interference and signal loss in deep tissues, which reduce image quality and diagnostic accuracy. Improving image quality remains a key focus of current research.

In a study by Muhammad Nasir Khan *et al.* [12], several filters — including median, mean, and Lee filters — were applied to ultrasound images of soft tissue to remove speckle noise. RMSE and PSNR were used to evaluate performance. However, this study did not address other random noise sources that also affect image quality.

According to J. Civale et al. [13], high frequencies (500–1000 Hz) can provide higher-quality elastography images due to their better spatial resolution; however, as the frequency increases, the attenuation of shear waves also becomes higher, causing significant energy attenuation and reduced image quality in deeper tissues [14-15]. In contrast, lower frequencies allow shear waves to propagate deeper into the tissue because of slower energy attenuation, but they decrease the spatial resolution and sharpness of the elastography images [16]

Recently, Abbassian Ardakani *et al.* [17] introduced a deep learning–based filter named AdaRes, which uses adaptive residual learning to reduce speckle and Gaussian noise in ultrasound images. The results showed that AdaRes could effectively remove different types of noise without changing the tissue structure, while keeping important image features and improving tumor classification accuracy (the median AUC increased from 0.494 to 0.702). However, like many deep learning approaches, this method needs large and diverse training datasets as well as high computing power, which makes it difficult to use in real-time clinical applications.

In another study, Max Denis *et al.* [18] CUSE - a shear elastography method that utilizes a comb-shaped acoustic radiation force to generate multiple shear waves within a single scan - was used, which uses a comb-shaped acoustic radiation pattern to generate shear waves in a single scan. This method provides fast imaging and high accuracy, but it's only suitable for moderate depths - its accuracy decreases for deeper tissues.

This study enhances deep-tissue elastography by combining multi-point excitation with adaptive noise filtering. Two excitation points are activated sequentially to avoid interference or resonance noise, improving image quality and diagnostic reliability. Quantitative evaluation using RMSE and Q-index shows reduced noise and more consistent diagnostic results. RMSE measures numerical accuracy, while Q-index evaluates structural and contrast preservation. Together, these metrics confirm that the method reduces error while maintaining image fidelity, strengthening overall reliability.

2. MATERIALS AND METHODS

2.1. Tissue stiffness

The stiffness of the tissue is determined by the following equation:

$$E = \frac{s}{e} \tag{1}$$

Where: s is the compressive stress (applied force per unit area), e is the strain (relative deformation of the tissue), E is the Young's modulus**,** representing the tissue stiffness**.** Diseased tissue is stiffer than healthy tissue, with malignant tumors much stiffer than benign ones. Therefore, tissue stiffness is important for early cancer detection. Shear wave velocity (1–10 m/s) mainly indicates tissue elasticity. Biological tissues have a density near 1000 kg/m³, and their stiffness varies with tissue type and pathology. The relationship is given by the following equation:

$$E = 3\lambda c^2 \tag{2}$$

where λ is the tissue density, c is the shear wave velocity, and E is the elasticity.

2.2. Initialization and measurement of shear wave velocity

In this study, a vibrating needle was used to generate shear waves (Figure 1). This approach allows accurate control of the target region and easy adjustment of vibration amplitude and frequency to match tissue properties. When applied to the skin surface, the vibrations generate shear waves that travel perpendicular to the needle motion. A Doppler ultrasound system then measures the shear wave velocity to estimate tissue elasticity and viscosity.

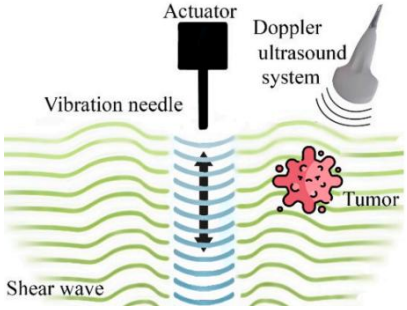

Figure 1. *Shear wave generation using a vibrating needle.*

Numerical simulation of shear wave propagation

The Finite-Difference Time-Domain (FDTD) method [19–21] was applied to simulate shear wave propagation in space. This method offers advantages over traditional wave equation approaches, as it can be applied to inhomogeneous media (e.g., tissues containing tumors). In this study, the investigated tissue was assumed to be linear and isotropic, which is a common and reasonable assumption for soft biological tissues under small deformations.The CSM, which consists of elastic and viscous components, represents the properties of the tissue. The Kelvin-Voigt model describes these viscoelastic characteristics and is expressed by equation (3).

$$\mathrm{M}(x, y, \omega) = \alpha(x, y) - i\omega\beta(x, y) \tag{3}$$

$\alpha(x,y)$ represents the elastic component of the tissue, while $\beta(x,y)$ represents the viscous component of the tissue in the spatial domain (x,y). The relationship between shear wave speed and the Complex Shear Modulus (CSM) is given in equations (4) - (6).

$$\lambda\partial_t v_z = \partial_x \sigma_{zx} + \partial_y \sigma_{zy} \tag{4}$$

$$\partial_t \sigma_{zx} = (\alpha + \beta\partial_t)\partial_x v_z \tag{5}$$

$$\partial_t \sigma_{zy} = (\alpha + \beta\partial_t)\partial_y v_z \tag{6}$$

The terms v_x and v_y represent the particle velocity components along the x and y directions, respectively, while σ_{zx} and σ_{zy} denote the corresponding components of the stress field. The symbol λ refers to the tissue density. The operator ∂_t denotes the partial derivative with respect to time t, and ∂_x and ∂_y indicate the partial derivatives with respect to the spatial coordinates x and y, respectively.

$$v_z^{\,n+1}|_{i,j} = v_z^{\,n}|_{i,j} + \frac{\Delta_t}{\lambda\Delta_x}\left(\sigma_{zx}^{\,n+\frac{1}{2}}|_{i+\frac{1}{2},j} - \sigma_{zx}^{\,n+\frac{1}{2}}|_{i-\frac{1}{2},j}\right) + \frac{\Delta_t}{\lambda\Delta_y}\left(\sigma_{zy}^{\,n+\frac{1}{2}}|_{i+\frac{1}{2},j} - \sigma_{zy}^{\,n+\frac{1}{2}}|_{i-\frac{1}{2},j}\right) \tag{7}$$

$$\sigma_{zx}^{\,n+1}|_{i+\frac{1}{2},j} = \sigma_{zx}^{\,n-\frac{1}{2}}|_{i+\frac{1}{2},j} + \frac{\alpha\Delta_t}{\Delta_x}\left(v_z^{\,n+1}|_{i+1,j} - v_z^{\,n+1}|_{i,j}\right) + \frac{\beta}{\Delta_x}\left(v_z^{\,n+1}|_{i+1,j} - v_z^{\,n+1}|_{i,j}\right) - \frac{\beta}{\Delta_x}\left(v_z^{\,n}|_{i+1,j} - v_z^{\,n}|_{i,j}\right) \tag{8}$$

$$\sigma_{zy}^{n+1}\Big|_{i+\frac{1}{2},j} = \sigma_{zx}^{n-\frac{1}{2}}\Big|_{i+\frac{1}{2},j} + \frac{\alpha\Delta_t}{\Delta_y}\left(v_z^{n+1}\big|_{i+1,j} - v_z^{n+1}\big|_{i,j}\right) + \frac{\beta}{\Delta_y}\left(v_z^{n+1}\big|_{i+1,j} - v_z^{n+1}\big|_{i,j}\right) - \frac{\beta}{\Delta_y}\left(v_z^{n}\big|_{i+1,j} - v_z^{n}\big|_{i,j}\right) \quad (9)$$

Equations (7), (8) and (9) were derived by applying the Finite-Difference Time-Domain (FDTD) method to equations (4), (5) and (6). where Δ_x and Δ_y represent the spatial intervals between consecutive positions along the x-axis and y-axis, respectively. Δ_t denotes the sampling period, *i* and *j* are the spatial indices along the x and y directions, and *n* is the time-step index.

2.3. System workflow

Figure 2 illustrates the workflow of the proposed data processing, detailing the filtering and preprocessing steps implemented to suppress noise, improve SNR, and enhance the quality of elasticity and viscosity images in deep tissue.

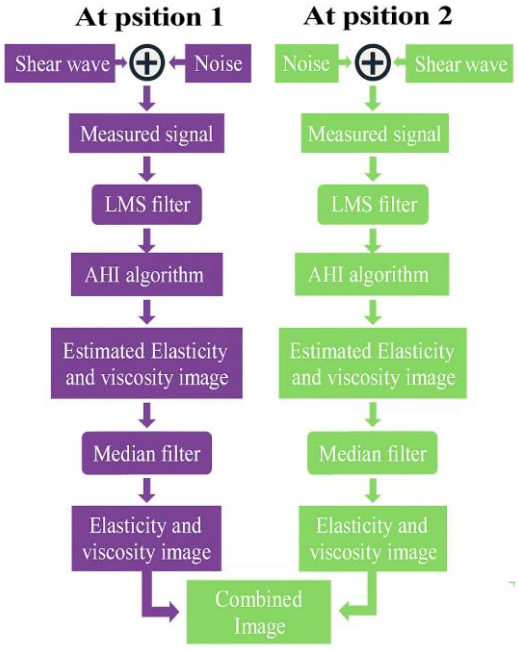

Figure 2. *The workflow.*

The workflow consists of several steps (Figure 2): first, the shear wave velocity signals are filtered using the LMS algorithm to remove random noise. The AHI algorithm is applied to estimate the elasticity and viscosity maps from the filtered signals [19, 23]. The resulting images are then processed with a median filter to reduce speckle noise [24]. Finally, the two images obtained from excitation positions 1 and 2 are combined to produce a composite image that represents the tissue's elasticity and viscosity.

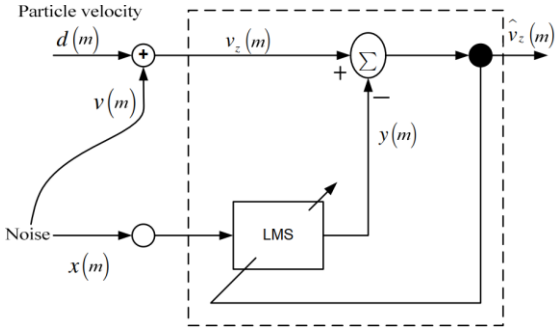

Figure 3. *Operation process of the least mean square filter.*

LMS Filter

Gaussian noise *v(n),* which reduces image quality, was added to the ideal signal. The ideal velocity *d(n)* at each spatial position was obtained from equations (4), (5), and (6). As illustrated in Figure 3, the LMS filter effectively suppressed the influence of the Gaussian noise.

Algorithm 1: Noise reduction using the LMS filter

1) Parameter Initialization:

Select the step size μ^*, define the filter length, and specify the noise variance.

2) Filter Initialization:

Set the initial filter coefficients to zero:

$w(0)=0$

3) Iterative Processing (for m=0,1,2,…):

a) **Compute the filter output:**

$y(m)=w(m)x(m)$

b) **Compute the error between the desired and estimated signals:**

$e(m)=v_z(m)-y(m)$

c) **Update the filter coefficients:**

$w(m+1)=w(m)+\mu e(m)x(m)$

d) **calculate the fltered signal by convolution**

4) Repeat **the above steps until the entire signal has been processed.**

Estimation of Tissue Elasticity and Viscosity Using the AHI Algorithm

The AHI algorithm estimated the tissue's elasticity and viscosity. based on the measured particle velocity values of the shear waves. Elasticity and viscosity are estimated using the equations presented in (10) and (11).

$$\alpha(x,y)=\mathrm{R}\left\{\frac{-\lambda\omega_0^{\,2}V_z(x,y,\omega_0)}{\nabla^2 V_z(x,y,\omega_0)}\right\} \tag{10}$$

$$\beta(x,y)=\mathrm{I}\left\{\frac{-\lambda\omega_0 V_z(x,y,\omega_0)}{\nabla^2 V_z(x,y,\omega_0)}\right\} \tag{11}$$

$V_z(x, y, \omega_0)$ was determined using the Fourier transform at the angular frequency ω_0. The operator $\nabla^2 V_z(x, y, \omega_0)$ was computed using the discrete Laplace function, denoted as $del2(V_z(x, y, \omega_0))$. This function provides a discrete approximation of the Laplacian when applied to $V_z(x, y,\omega_0)$.

Median Filter

Speckle noise commonly reduces ultrasound image quality. To address this issue, a 3×3 median filter was used in this study to reduce noise within the region of interest. For each window, the central pixel was replaced with the median value of the surrounding pixels. By applying this procedure across the entire image, noise was minimized while key structural features were protected.

Algorithm 2: Speckle noise reduction using a median filter

1) Obtain the dimensions of the input image (*height* and *width*).

2) Iterate over each pixel position *(i,j)* in the image:

Let i range from 2 to *height−1*

For each *i*, let *j* range from 2 to *width−1*

3) For each pixel, extract a 3×3 neighborhood centered at *(i,j)* and store the intensity values.

4) Sort the collected values in ascending order.

5) Replace the central pixel with the median value from the sorted list.

6) Repeat this procedure for all valid pixels to produce the noise-reduced image.

Simulation scenario

Shear wave propagation was modeled using the FDTD method with a 150 Hz excitation frequency and a 6 mm oscillation amplitude. A 20 mm tumor was placed at the center, and the ideal 2D elasticity and viscosity images are shown in Figure 4. The simulation was then repeated under noisy conditions with an SNR of 29.

Table 1. *tissue properties.*

Tissue Type	Viscosity (Pa·s)	Elasticity (Pa)
Pathological tissue	1.8	9000
Normal tissue tissue	1.2	6000

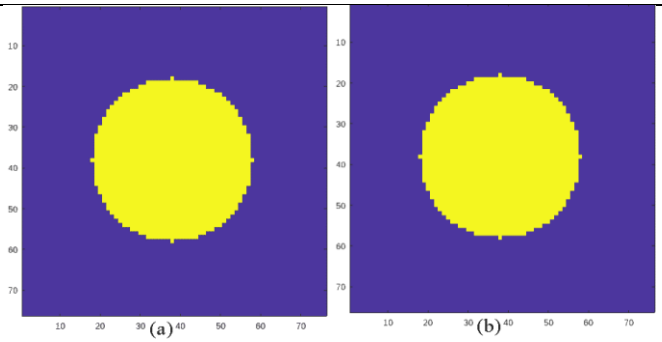

Figure 4. *Ideal elasticity (a) and viscosity (b) images.*

3. RESULTS AND DISCUSSION

Source at Position 1

The excitation source at position (40,0) generated shear waves that propagated rightward toward the tumor, with amplitude decreasing as the waves moved farther from the source. Shear wave velocity was then used to estimate tissue elasticity and viscosity via the AHI algorithm, after applying LMS and median filters to the signals. The reconstructed 2D images show that the tumor's shape, size, and location closely match the ideal image. However, noise increases toward the right side due to wave energy attenuation with distance (Figure 5).

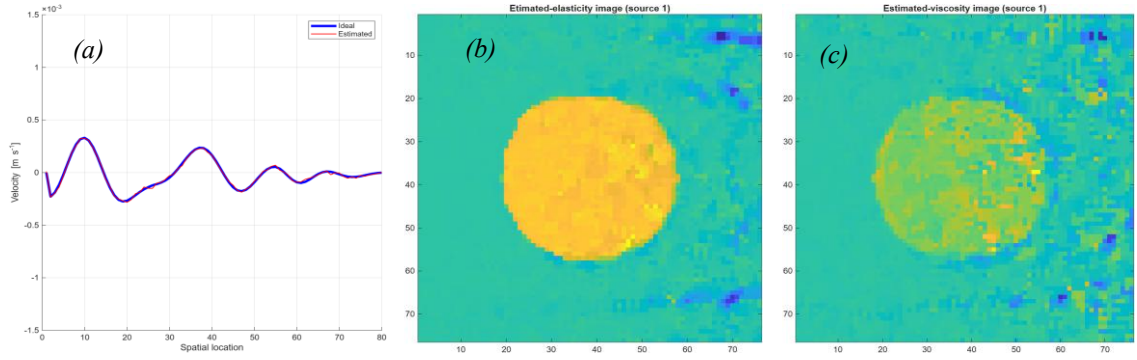

Figure 5. *a) Shear wave velocity b) Elasticity and c) Viscosity images.*

Figure 6 shows that the estimated elasticity and viscosity match the ideal values near the excitation source. However, with increasing distance, the estimated curve fluctuates more and deviates from the reference due to shear wave energy attenuation, which lowers the SNR in deeper regions.

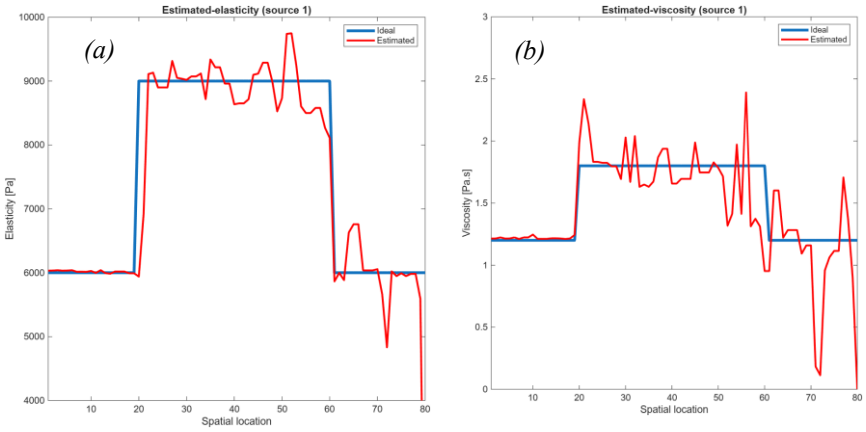

Figure 6. *Elasticity (a) and viscosity (b) profiles along line 40.*

Source at Position 2

At position (40,80), the excitation source was placed to the right of the tumor, generating shear waves that propagated leftward. Noise increased with distance from the source, causing a gradual decline in image quality (Figure 7).

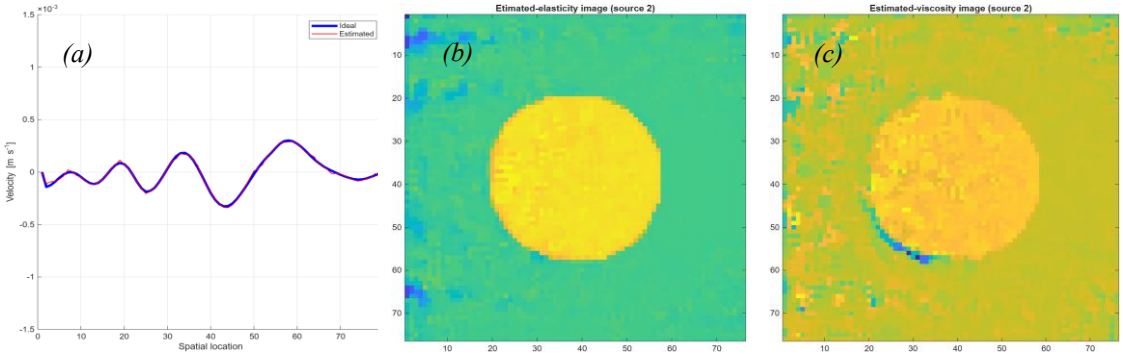

Figure 7. *a) Shear wave velocity b) Elasticity and c)Viscosity images.*

The 1D estimated elasticity and viscosity curves along line 40 (Figure 8) closely match the ideal curves on the right side, near the excitation source. However, as the distance increases, the estimated curves show stronger fluctuations and deviate further from the ideal ones.

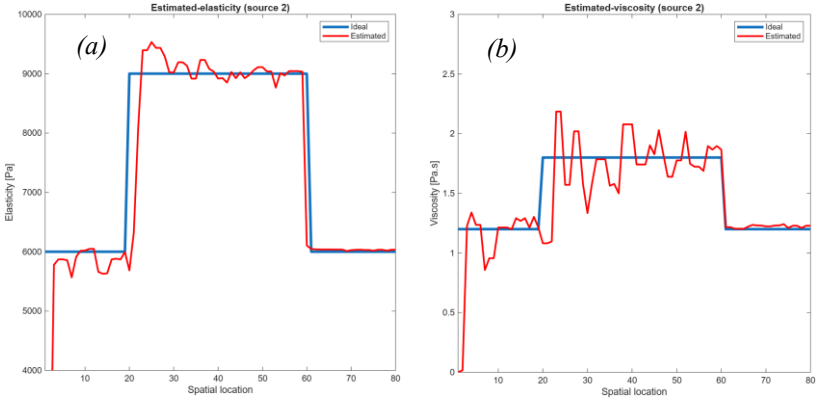

Figure 8. *Elasticity (a) and viscosity (b) graphs along line 40.*

Combination of Source 1 and Source 2

The combined-source 2D elasticity and viscosity images (Figure 9) show **significantly** less noise than those reconstructed from each source individually.

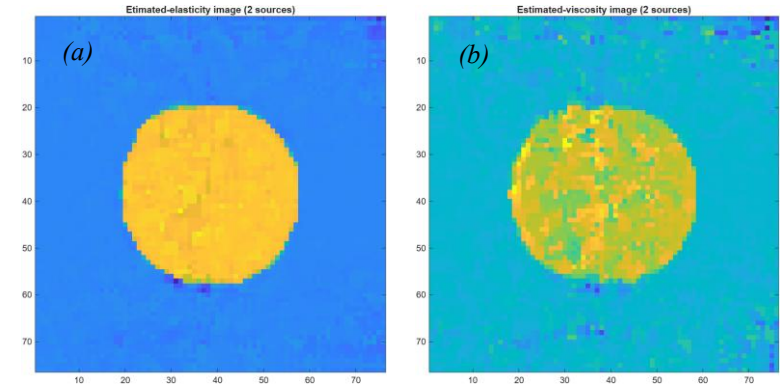

Figure 9. *Elasticity (a) and viscosity (b) images after combination.*

The combined 1D elasticity and viscosity graphs along line 40 (Figure 10) show improved results, effectively reducing noise in regions far from the excitation sources.

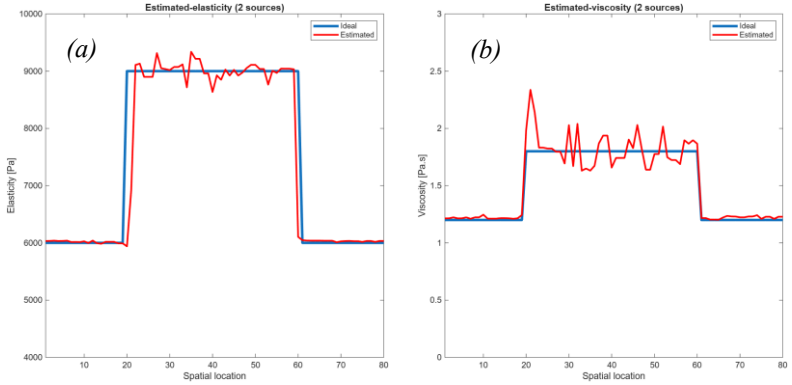

Figure 10. *Combined elasticity (a) and viscosity (b) graphs.*

Q-Index

To compare the similarity between two images, the *Q-Index* is employed, which takes into account three visual perception factors: luminance, contrast, and structural information [26]. The *Q-Index* ranges from -1 to 1, where a value of 1 represents complete similarity between the images. Let *(I)* be the ideal reference image of size *(M x N),* and *(K)* be the estimated image

$$\mathbf{Q} = \frac{\mathbf{4\sigma_{xy}\overline{x}\,\overline{y}}}{(\mathbf{\sigma_x^2 + \sigma_y^2})(\mathbf{\overline{x}^2 + \overline{y}^2})} \qquad (12)$$

$$\mathbf{\overline{x}} = \frac{\mathbf{1}}{\mathbf{MN}} \sum_{\mathbf{i=1}}^{\mathbf{M}} \sum_{\mathbf{j=1}}^{\mathbf{N}} \mathbf{I(i,j)} \qquad (13)$$

$$\mathbf{\overline{y}} = \frac{\mathbf{1}}{\mathbf{MN}} \sum_{\mathbf{i=1}}^{\mathbf{M}} \sum_{\mathbf{j=1}}^{\mathbf{N}} \mathbf{K(i,j)} \qquad (14)$$

$$\sigma_{xy} = \frac{1}{MN-1} \sum_{i=1}^{M} \sum_{j=1}^{N} (I(i,j) - \overline{x})(K(i,j) - \overline{y}) \qquad (15)$$

Where $\bar{x}$ is the mean intensity of image *I* and $\bar{y}$ is the mean intensity of image *K*. σ_x^2 and σ_y^2 represent the variance values of images *(I)* and *(K),* indicating their contrast and the degree of pixel intensity variation. Higher contrast improves the ability to identify structural details and boundary edges in the image.

Figure 11 illustrates the relationship between the *Q-Index* and SNR for the elasticity and viscosity images. The blue, black, and red curves correspond to the combined image, source 2, and source 1, respectively. A *Q-Index* value closer to 1 reflects higher image similarity. As observed, the blue curve remains the highest and nearest to 1, indicating that the combined image achieves a

closer match to the ideal image compared to using each source individually.

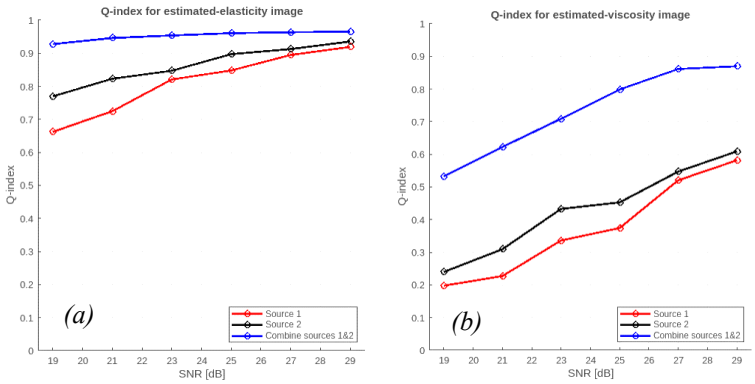

Figure 11. *a) Elasticity Q-Index and b) Viscosity Q-Index.*

RMSE (Root Mean Square Error)

A lower RMSE means the estimated image is closer to the ideal one. RMSE measures the difference between the two images. In this formulation, *(I)* refers to the reference image, *(K)* denotes the estimated image, and *(M x N)* specifies the image dimensions.

$$RMSE = \sqrt{\frac{1}{MN}\sum_{i=0}^{M-1}\sum_{j=0}^{N-1}[I(i,j)-K(i,j)]^2} \tag{16}$$

As illustrated in figure 12, the RMSE values for the combined elasticity and viscosity reconstructions (blue curves) are consistently lower than those derived from individual source excitations, indicating improved estimation accuracy.

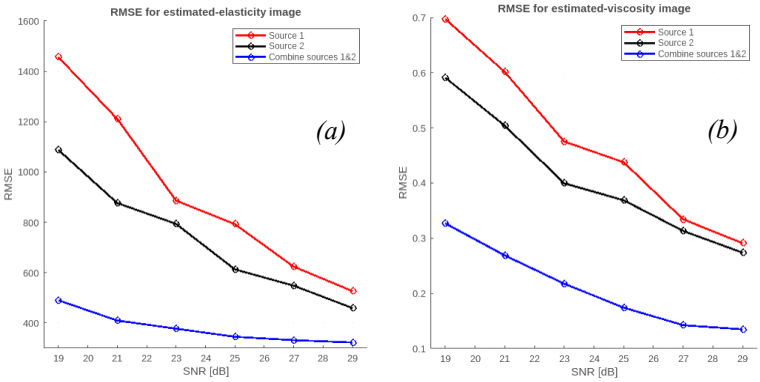

Figure 12. *a)Elasticity RMSE b) Viscosity RMSE.*

4. CONCLUSIONS

Compared with study [27], this thesis significantly improves the quality of elasticity and viscosity (CSM) images in deep tissue through advanced multi-stage noise suppression, dual-point excitation, and quantitative evaluation. Unlike [27], which applies only LMS filtering for Gaussian noise, the proposed framework effectively addresses speckle and structured noise while enhancing the shear wave field to improve SNR. Although dual-point excitation increases processing time compared to a single source, the overall simulation time remains acceptable (≈3 minutes on a personal computer and ≈1 minute on MATLAB Online), and the superiority of the method is confirmed by RMSE and Q-index. In future studies, we aim to improve elastography image quality in deep and heterogeneous tissues using directional filtering and to extend the method to three-dimensional imaging via shear wave velocity estimation in all spatial directions. The proposed

approach will be validated using real patient data and diverse clinical datasets with qualitative clinician assessment, while its diagnostic relevance and applicability to other organs and anatomically complex structures will be evaluated.

REFERENCES

[1]. Essue BM, Iragorri N, Fitzgerald N, de Oliveira C. *"The psychosocial cost burden of cancer: A systematic literature review"*. Psychooncology, vol. 29, no. 11, pp. 1746–1760, (2020). DOI: 10.1002/pon.5516.

[2]. Girgis A, Lambert S, Johnson C, Waller A, Currow D. *"Physical, psychosocial, relationship, and economic burden of caring for people with cancer: a review"*. J Oncol Pract, vol. 9, no. 4, pp. 197–202, (2013). DOI: 10.1200/JOP.2012.000690.

[3]. Li Z, Aninditha T, Griene B, Francis J, Renato P, Serrie A, Umareddy I, Boisseau S, Hadjiat Y. *"Burden of cancer pain in developing countries: a narrative literature review"*. Clinicoecon Outcomes Res, vol. 10, pp. 675–691, (2018). DOI: 10.2147/CEOR.S181192.

[4]. Bray F, Laversanne M, Sung H, Ferlay J, Siegel RL, Soerjomataram I, Jemal A. *"Global cancer statistics 2022: GLOBOCAN estimates of incidence and mortality worldwide for 36 cancers in 185 countries"*. CA Cancer J Clin, vol. 74, no. 3, pp. 229–263, (2024). DOI: 10.3322/caac.21834.

[5]. Homan SG, Yun S, Bouras A, Schmaltz C, Gwanfogbe P, Lucht J. *"Breast Cancer Population Screening Program Results in Early Detection and Reduced Treatment and Health Care Costs for Medicaid"*. J Public Health Manag Pract, vol. 27, no. 1, pp. 70–79, (2021). DOI: 10.1097/PHH.0000000000001041.

[6]. Chung KC, Muthutantri A, Goldsmith GG, Watts MR, Brown AE, Patrick DL. *"Symptom impact and health-related quality of life (HRQoL) assessment by cancer stage: a narrative literature review"*. BMC Cancer, vol. 24, no. 1, p. 884, (2024). DOI: 10.1186/s12885-024-12612-z.

[7]. Kim JH, Kim SS, Lee JH, Jung DH, Cheung DY, Chung WC, Park SH. *"Early Detection is Important to Reduce the Economic Burden of Gastric Cancer"*. J Gastric Cancer, vol. 18, no. 1, pp. 82-89, (2018). DOI: 10.5230/jgc.2018.18.e7.

[8]. Crosby D, Bhatia S, Brindle KM, Coussens LM, Dive C, Emberton M, Esener S, Fitzgerald RC, Gambhir SS, Kuhn P, Rebbeck TR, Balasubramanian S. *"Early detection of cancer"*. Science, vol. 375, no. 6586, p. eaay9040, (2022). DOI: 10.1126/science.aay9040.

[9]. Tang GX, Xiao XY, Xu XL, Yang HY, Cai YC, Liu XD, Tian J, Luo BM. *"Diagnostic value of ultrasound elastography for differentiation of benign and malignant axillary lymph nodes: a meta-analysis"*. Clin Radiol, vol. 75, no. 6, pp. 481.e9–481.e16, (2020). DOI: 10.1016/j.crad.2020.03.021.

[10]. Zhou Y, Chen H, Qiang J, Wang D. *"Systematic review and meta-analysis of ultrasonic elastography in the diagnosis of benign and malignant thyroid nodules"*. Gland Surg, vol. 10, no. 9, pp. 2734–2744, (2021). DOI: 10.21037/gs-21-492.

[11]. Selim YAY, Sabit H, Arneth B, Shaaban MA. *"Diagnostic Accuracy of Sonoelastography for Breast Lesions: A Meta-Analysis Comparing Strain and Shear Wave Elastography"*. J Imaging, vol. 11, no. 7, p. 221, (2025). DOI: 10.3390/jimaging11070221.

[12]. Khan MN, Altalbe A. *"Experimental evaluation of filters used for removing speckle noise and enhancing ultrasound image quality"*. Biomed Signal Process Control, vol. 73, p. 103399, (2022). DOI: 10.1016/j.bspc.2021.103399.

[13]. Huang C, Song P, Mellema DC, Gong P, Lok UW, Tang S, Ling W, Meixner DD, Urban MW, Manduca A, Greenleaf JF, Chen S. *"Three-dimensional shear wave elastography on conventional ultrasound scanners with external vibration"*. Phys Med Biol, vol. 65, no. 21, p. 215009, (2020). DOI: 10.1088/1361-6560/aba5ea.

[14]. Madsen EL, Sathoff HJ, Zagzebski JA. *"Ultrasonic shear wave properties of soft tissues and tissuelike materials"*. J Acoust Soc Am, vol. 74, no. 5, pp. 1346-55, (1983). DOI: 10.1121/1.390158.

[15]. Ploquin M, Basarab A, Kouamé D. *"Resolution enhancement in medical ultrasound imaging"*. J Med Imaging (Bellingham), vol. 2, no. 1, p. 017001, (2015). DOI: 10.1117/1.JMI.2.1.017001.

[16]. Neumann, D., Kollorz, E. *"Ultrasound"*. Medical Imaging Systems. Lecture Notes in Computer Science, vol. 11111, (2018). DOI: 10.1007/978-3-319-96520-8_11.

[17]. Abbasian Ardakani A, Mohammadi A, Vogl TJ, Kuzan TY, Acharya UR. *"AdaRes: A deep learning-based model for ultrasound image denoising: Results of image quality metrics, radiomics, artificial*

intelligence, and clinical studies". J Clin Ultrasound, vol. 52, no. 2, pp. 131–143, (2024). DOI: 10.1002/jcu.23607.
[18]. Denis M, Mehrmohammadi M, Song P, Meixner DD, Fazzio RT, Pruthi S, Whaley DH, Chen S, Fatemi M, Alizad A. *"Comb-push ultrasound shear elastography of breast masses: initial results show promise"*. PLoS One, vol. 10, no. 3, p. e0119398, (2015). DOI: 10.1371/journal.pone.0119398.
[19]. Luong QH, Nguyen SH, Tran DN, Nguyen CM, Tran DT. *"Viscoelastic Estimation of Soft Tissue in the Presence of Gaussian and Reflection Noises Impacting Shear Wave Propagation"*. Proc. 12th Int Conf Control, Automation and Information Sciences (ICCAIS), pp. 622–627, (2023). DOI: 10.1109/ICCAIS59597.2023.10382326.
[20]. Luong QH, Tran DN, Hiep NS, Cong LS, Tran DT. *"Enhancing Shear Wave Propagation Analysis in Tissue with Directional Filtering of Reflected Waves"*. Proc. Asia Pacific Signal and Information Processing Association Annual Summit and Conference (APSIPA ASC), pp. 1–6, (2024). DOI: 10.1109/APSIPAASC63619.2025.10848844.
[21]. Sheu YL, Li PC. *"Simulations of photoacoustic wave propagation using a finite-difference time-domain method with Berenger's perfectly matched layers"*. J Acoust Soc Am, vol. 124, no. 6, pp. 3471–3480, (2008). DOI: 10.1121/1.3003087.
[22]. Bojorjes AR, Garcia-Barrientos A, Cárdenas-Juárez M, Pineda-Rico U, Arce A, Velasquez SM, Cortés OP. *"A Z-Test-Based Evaluation of a Least Mean Square Filter for Noise Reduction"*. Acoustics, vol. 7, p. 20, (2025). DOI: 10.3390/acoustics7020020.
[23]. Kotropoulos C, Pitas I. *"Adaptive LMS filters for noise suppression in images"*. IEEE Trans Image Process, vol. 5, no. 12, pp. 1596–609, (1996). DOI: 10.1109/83.544568.
[24]. Naik VN, Gamad RS, Bansod PP. *"Effect of despeckling filters on the segmentation of ultrasound common carotid artery images"*. Biomed J, vol. 45, no. 4, pp. 686–695, (2022). DOI: 10.1016/j.bj.2021.07.002.
[25]. Shiao YH, Chen TJ, Chuang KS, Lin CH, Chuang CC. *"Quality of compressed medical images"*. J Digit Imaging, vol. 20, no. 2, pp. 149–59, (2007). DOI: 10.1007/s10278-007-9013-z.
[26]. Wang Z, Bovik AC. *"A universal image quality index"*. IEEE Signal Process Lett, vol. 9, no. 3, pp. 81–84, (2002). DOI: 10.1109/97.995823.
[27]. Pham-Thi TH, Luong QH, Nguyen VD, Tran DT, Huynh HT. *"Two-dimensional complex shear modulus imaging of soft tissues by integration of Algebraic Helmoltz Inversion and LMS filter into dealing with noisy data: a simulation study"*. Math Biosci Eng, vol. 17, no. 1, pp. 404-417, (2019). DOI: 10.3934/mbe.2020022.

TÓM TẮT

KelvinVoigt – Kích thích đa điểm: Mô hình hiệu quả nâng cao chất lượng ảnh đàn hồi trong mô sâu

Độ cứng mô là chỉ số quan trọng cho biết tình trạng bệnh lý của cơ thể. Kỹ thuật Siêu âm đàn hồi mô dựa trên đặc tính cơ học của mô giúp chẩn đoán nhiều bệnh như ung thư vú, tuyến giáp, tuyến tiền liệt, hiệu quả với ưu điểm nhanh, chi phí thấp, không xâm lấn và đáng tin cậy. với những ưu điểm trên, kỹ thuật siêu âm đàn hồi mô đang được quan tâm và sử dụng rộng rãi trong chẩn đoán lâm sàng. Tuy nhiên, kĩ thuật cũng gặp phải những bất lợi khi nhiễu xuất hiện nhiều ở những vùng mô sâu gây suy giảm chất lượng ảnh và làm giảm độ chính xác chẩn đoán. Nghiên cứu này đề xuất tích hợp lọc LMS, lọc trung vị và tăng cường nguồn kích thích đa vị trí nhằm cải thiện SNR và tăng cường chất lượng ảnh ở vùng mô sâu. Hiệu quả của phương pháp được đánh giá qua hai chỉ số RMSE và Q-index, cho thấy giảm nhiễu rõ rệt và nâng cao độ tin cậy trong chẩn đoán.

Từ khoá: Thuật toán AHI; Bộ lọc LMS; Ảnh đàn hồi mô; Lọc trung vị; Kích thích đa điểm.